Mechanical Systems and Signal Processing 81 (2016) 43–59

Contents lists available at ScienceDirect

Mechanical Systems and Signal Processing

journal homepage: www.elsevier.com/locate/ymssp

Reconfiguration of a four-bar mechanism using phase space connections

Jiaying Zhang [a,b,*], Colin R. McInnes [b]

[a] Department of Mechanical and Aerospace Engineering, University of Strathclyde, Glasgow G1 1XJ, United Kingdom
[b] School of Engineering, University of Glasgow, Glasgow G12 8QQ, United Kingdom

ARTICLE INFO

Article history:
Received 29 September 2015
Received in revised form
29 March 2016
Accepted 31 March 2016
Available online 6 April 2016

Keywords:
Reconfiguration
A four-bar mechanism
Heteroclinic connections
Instability
Active control

ABSTRACT

Linkage mechanisms are perhaps the simplest mechanical structures in engineering, but they can exhibit significant nonlinearity which can in principle be exploited. In this paper a simple smart structure model is developed based on such nonlinearity to investigate the reconfiguration of a four-bar mechanism through phase space connections. The central idea is based on heteroclinic connections in the mechanism phase space between equal-energy unstable equilibria. It is proposed that transitions between such equal-energy unstable (but actively controlled) equilibria in principle require zero net energy input, compared to transitions between stable equilibria which require the input and then dissipation of energy. However, it can be difficult to obtain such heteroclinic connections numerically in complex dynamical systems, therefore an objective function approach is used to seek transitions between unstable equilibria which approximate true heteroclinic connections. The instability inherent in the model is therefore actively utilised to provide energy-efficient transitions between configurations of the mechanism. It will be shown that the four-bar mechanism then forms the basis for an elastic model of a smart buckling beam.

1. Introduction

A linkage mechanism is a simple mechanical device with the purpose of transferring force from an input to an output [1]. Some mechanisms have been developed that possess two or more equilibrium configurations, so-called bistable and tristable mechanisms. These mechanisms use external energy input to transition from one stable position to other stable positions over a potential energy barrier [2,3]. Such ingenious mechanisms have broad application in practical engineering, and research continues to improve their performance [4]. Meanwhile, multiple equilibria are widespread in a range of other phenomenon, not only those involved in mechanical processes but also ranging from electronics to living cells. These systems have the fundamental feature that once an input reaches a certain threshold value, the system switches to and stays in the corresponding state even when the input is removed [5,6].

The theory of mechanisms with multiple equilibria can be employed to investigate practical structures, such as a continuous elastic bistable beam model that has been developed by Camescasse et. al [7]. Nonlinear theory was firstly used to analyse a numerical model and then employed to verify the validity of the proposed continuous model [8]. Cleary and Su

* Corresponding author at: Department of Mechanical and Aerospace Engineering, University of Strathclyde, Glasgow G1 1XJ, United Kingdom.
E-mail address: jiaying.zhang@strath.ac.uk (J. Zhang).

http://dx.doi.org/10.1016/j.ymssp.2016.03.024
0888-3270/

have considered that a bistable buckled beam can be actuated by a moment input and proved that their theoretical model provides guidelines to design bistable compliant mechanisms [9]. Others have been inspired by origami design principles and natural phenomenon to develop bistable geometries [10] and so delivered a morphing process which can reduce the amount of external work to deploy a morphing structure [11]. Meanwhile smart materials, which can change their properties under external stimuli such as stress, temperature, electric or magnetic fields, for example shape memory materials (SMM) [12], can be used to design and manufacture smart structures [13]. Hogg and Huberman have investigated active control of such structures comprised of smart materials using an agent-based approach [14]. More recently a new smart structure concept has been presented, which can fold itself into a desire shape with embedded sensors and actuators [15].

In previous related work, McInnes and Waters considered reconfiguration of smart structures using phase space connections [16]. A simple smart structure model was presented, constructed from two masses and three springs clamped at both ends. The model was approximated with cubic nonlinearities to investigate the key characteristics of the system. A set of both stable and unstable equilibrium configurations were identified with a subset of equal-energy unstable configurations found. A novel method was then proposed to reconfigure the smart structure between these equal-energy unstable states using heteroclinic connections in the phase space of the problem. It was assumed that active control could maintain the structure in each unstable state [17]. This cubic nonlinear model has also been used to investigate vibrational energy harvesting through the use of stochastic resonance [18].

A reconfigurable smart model is considered here as a mechanical system which has the ability to change its kinematic configuration between a finite set of stable or unstable equilibria. Heteroclinic connections are then employed to achieve a reconfiguration of the structure by connecting the unstable equilibria that lie on the same energy surface in the phase space of the problem. In principle, zero net energy is required to achieve transition between these unstable equilibria, unlike transitions between stable equilibria which require the addition of and then dissipation of energy [16]. Moreover, a computational optimal control method can be used to determine the required control time histories under a set of desired boundary conditions with a suitable performance index function [19]. In addition, a reconfiguration method based on a reference trajectory and an inverse control method has been applied to a simple double mass-spring model of a smart structure [20].

In this paper, a classical four-bar mechanism with rigid linkages and torsional springs is firstly investigated. The rigid model demonstrates the possibility of reconfiguring the mechanism between two unstable equilibria. Moreover, the rigid four-bar mechanism allows a simple controller to be developed to actively stabilise the unstable configurations of the structure. Then, a single axial spring is used to substitute for one rigid bar to develop a pseudo-rigid model, which illustrates interesting complexities over the rigid model. An approximation of the trigonometric terms in the governing equations is then used to construct a simple mathematical model which is employed to illustrate the calculation of heteroclinic connections and active control.

Lastly, a purely elastic model with torsional springs and axial springs for linkages is developed which allows bending, stretching and compression. An energy-based method is used to verify the fidelity of the model relative to a flexible buckling beam. The paper therefore uses the four-bar mechanism and intermediate pseudo-rigid model as a means of developing a model of an actively controlled buckling beam. The fundamental properties of the flexible model are then discussed using nonlinear systems theory to determine which equilibria can be connected through the phase space of the problem. In particular, paths in the phase space which join an equilibrium point to itself (homoclinic connections) and two different equilibrium point (heteroclinic connections) are sought. Again, heteroclinic connections are considered as a means of enabling energy-efficient transitions between unstable configurations of the reconfigurable elastic structure. Some numerical results are then presented to elaborate on the feasibility of this reconfiguration manoeuvre.

2. Rigid four-bar model

The motion of a link mechanism can be modelled using standard kinematic equations, which can be derived from Ref.

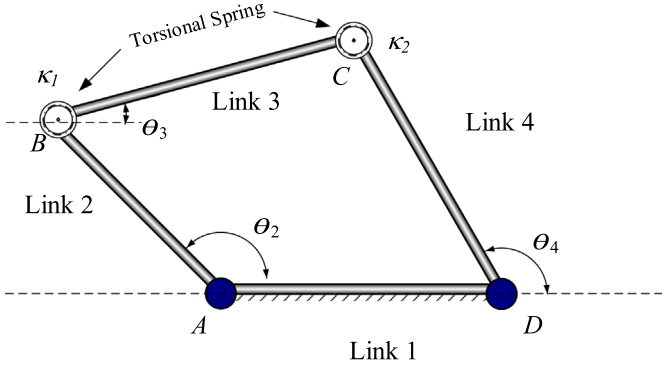

Fig. 1. Four-bar mechanism with torsional springs model.

Table 1
Properties of the four-bar mechanism model.

Variable	Value	Description
r_1	12.70 (cm)	Link 1 length
r_2	13.97 (cm)	Link 2 length
r_3	13.97 (cm)	Link 3 length
r_4	13.97 (cm)	Link 4 length
κ_1	0.164 (N-m/rad)	Spring constant
κ_2	0.164 (N-m/rad)	Spring constant

[1]. A four-bar linkage is a basic mechanism which has only one degree of freedom, as shown in Fig. 1. The properties of this mechanism, such as range of movement, is based on the link lengths. In this paper, the nonlinearity of a four-bar linkage is discussed with specified dimensions, listed in Table 1, which were used in Ref. [3]. The input link can be chosen as link 2, link 3 or link 4, however, link 3 is selected here as the input link. Joint 2 and joint 3 are then assumed to have ideal torsional springs so that the system can be considered as conservative without friction. Therefore, the torsional springs can store or release energy when the mechanism moves. This re-distribution of (conserved) energy provides one or more distinct equilibrium positions (both stable and unstable), which is the basis for the following analysis on reconfiguration. The initial configuration of the mechanism is that link 3 is parallel to link 1, denoted by θ_3=0. Following the development of Ref. [2] the energy of the system can then be found from

$$V = \sum_{0}^{n} \frac{1}{2}\kappa_i \psi_i^2 \tag{1}$$

where n is the numbers of torsional springs, V is the potential energy of the system, κ_i is the torsional spring constant of ith torsional spring and ψ_i is the angle of deflection of the bar. For each angle of deflection of the specific system shown in Fig. 1 it can be seen that

$$\begin{aligned} \psi_2 &= (\theta_3 - \theta_{30}) - (\theta_2 - \theta_{20}) \\ \psi_3 &= (\theta_4 - \theta_{40}) - (\theta_3 - \theta_{30}) \end{aligned} \tag{2}$$

where the subscript'0' indicates the initial angle of the rigid bar and link 1 is fixed in the horizontal direction as shown in Fig. 1. The total potential energy of the mechanism based on two torsional springs at joint 2 and joint 3 can then be written as

$$V = \frac{1}{2}\kappa_1 \psi_2^2 + \frac{1}{2}\kappa_2 \psi_3^2 \tag{3}$$

The moments required to keep the mechanism in a particular position can be obtained through the principle of virtual work [21]. The moment can be considered as the first derivative of the potential energy function with respect to the angle of the input link, so that the potential energy can be considered as

$$V = \int_{\theta_0}^{\theta} M d\theta \tag{4}$$

and by considering link 3 as the input link, then taking the derivative of Eq. (4) the moment M_3 is found from

$$M_3 = \frac{dV}{d\theta_3} \tag{5}$$

The initial configuration of the mechanism is that link 3 is parallel to link 1, i.e. θ_{30}=0. Therefore, the moment defined by Eq. (5) can be rewritten as

$$M_3 = \kappa_1 \psi_2 \frac{d\psi_2}{d\theta_3} + \kappa_2 \psi_3 \frac{d\psi_3}{d\theta_3} \tag{6}$$

Using the kinematics of the link mechanism [1], the derivatives in Eq. (6) can be expressed using the additional relationships

$$\frac{d\theta_2}{d\theta_3} = \frac{r_3 \sin(\theta_3 - \theta_4)}{r_2 \sin(\theta_4 - \theta_2)} \tag{7}$$

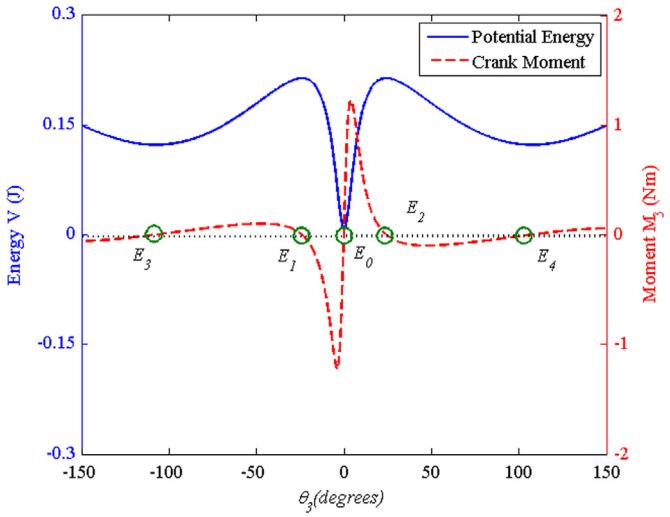

Fig. 2. Energy and moment for the rigid four-bar mechanism.

and

$$\frac{d\theta_4}{d\theta_2}=\frac{r_4 \sin(\theta_4-\theta_2)}{r_3 \sin(\theta_3-\theta_2)} \tag{8}$$

The equilibrium positions of the mechanism can then be determined from the first derivative of the total potential energy when it is null. The stability of these equilibrium positions can also be determined by considering the sign of the second derivate of the potential energy. Any positions corresponding to local minima (local maxima) are stable (unstable) equilibrium points.

Some characteristics of the system will now be considered. The dimensions of four-bar mechanism model are again shown in Table 1, where the model is a symmetric system with torsional springs at joints B and C only. The total potential energy of the torsional springs is shown in Fig. 2. It can be seen that there are two unstable equilibrium positions and three stable equilibrium positions in this symmetric model, listed in Table 2. The corresponding shape of the four-bar mechanism can be seen in Fig. 3, which shows one torsional spring in compression while the other is extended in the unstable equilibrium positions.

In addition, a bifurcation diagram can be constructed through using different ratios between κ_1 and κ_2, as shown in Fig. 4. Again, the number and position of the equilibria can be modified based on the free parameters of system.

A transition from E_1 to E_2 is now considered as an example to illustrate the method whereby equal-energy unstable configurations can be connected. The model is again considered to be a conservative system with the simplification that it has unit mass. We can now define the problem by a dynamical system of the form

$$\dot{\theta}_3=\omega_3 \tag{9}$$

$$\dot{\omega}_3=\kappa_1\psi_2\frac{d\psi_2}{d\theta_3}+\kappa_2\psi_3\frac{d\psi_3}{d\theta_3} \tag{10}$$

Due to numerical error (and practically since the transition is between unstable equilibria) active control is required, which captures trajectories in a neighbourhood of E_2. The system has only one degree of freedom, so that only a simple controller is required. Here, the torsional spring at joint 3 is used as a controller, where it is assumed that the spring is fabricated from a suitable material, such as a shape memory alloy. In order to ensure convergence to some required equilibrium point $\tilde{\theta}_3$ a Lyapunov function [22] will be defined as

$$\phi(\theta_3, \omega_3)=\frac{1}{2}\omega_3^2+\frac{1}{2}(\theta_3-\tilde{\theta}_3)^2 \tag{11}$$

Table 2
Equilibrium points and corresponding potential energy.

Point	θ_3 (deg)	V (Potential)	Type
E_0	0	0	Stable
E_1	−26.83	0.21844	Unstable
E_2	26.83	0.21844	Unstable
E_4	−92.60	0.1687	Stable
E_5	92.60	0.1687	Stable

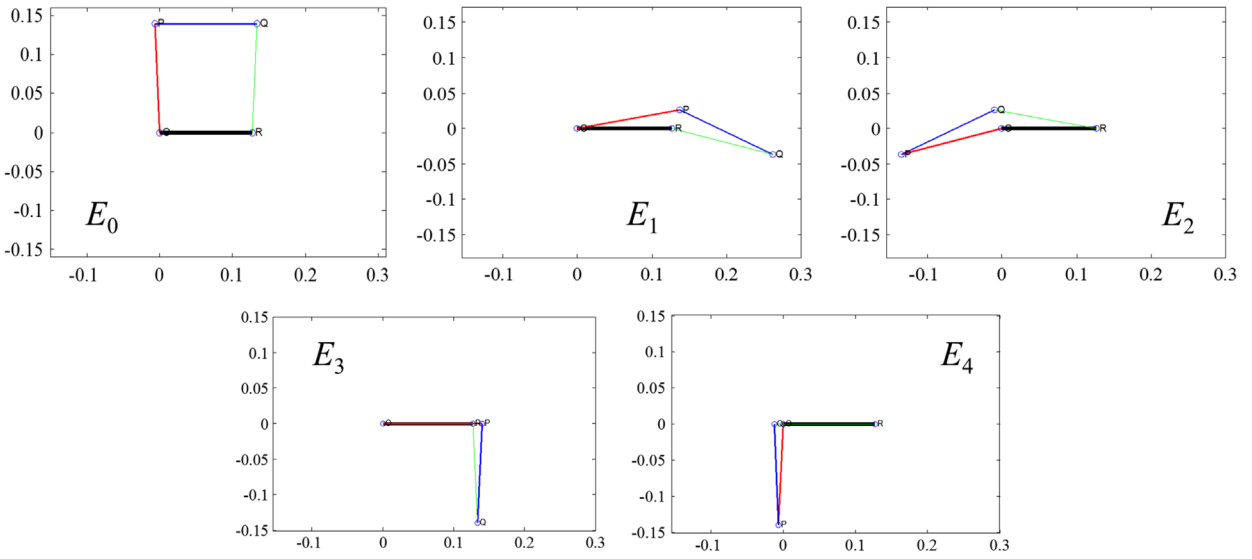

Fig. 3. Shape of the four-bar mechanism in equilibrium positions.

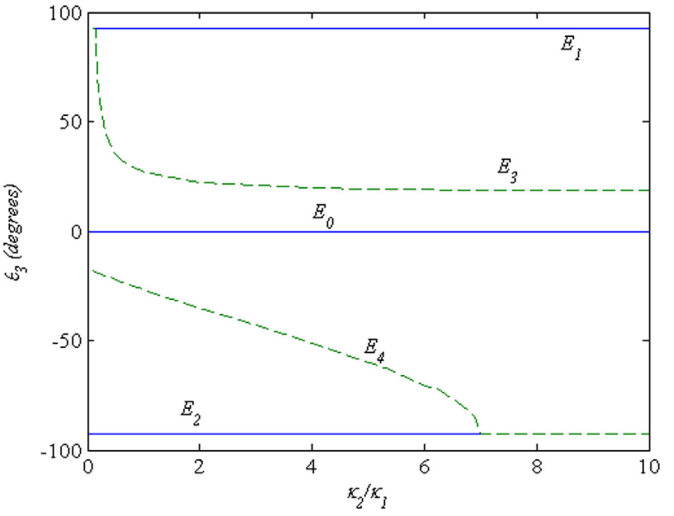

Fig. 4. Bifurcation diagram for the four-bar mechanism, solid line: stable equilibria, dashed line: unstable equilibria.

where $\phi(\theta_3, \omega_3)>0$ and $\phi(\tilde{\theta}_3,0)=0$. The time derivative of the Lyapunov function is clearly

$$\dot{\phi}(\theta_3, \omega_3)=\omega_3\left(\dot{\omega}_3+\left(\theta_3-\tilde{\theta}_3\right)\right) \tag{12}$$

Then, substituting from the Eq. (10) the controller for $\kappa_2$can be defined as

$$\kappa_2=-\frac{1}{\psi_3\frac{d\psi_3}{d\theta_3}}\left(\kappa_1\psi_2\frac{d\psi_2}{d\theta_3}+\eta\omega_3+\left(\theta_3-\tilde{\theta}_3\right)\right) \tag{13}$$

for some control parameter η. It is noted that $\psi_3\frac{d\psi_3}{d\theta_3}\neq 0$ in the neighbourhood of the required equilibrium point $\tilde{\theta}_3$. It can then be seen that ϕ is monotonically decreasing such that

$$\dot{\phi}(\theta_3, \omega_3)=-\eta\omega_3^2\leq 0 \tag{14}$$

and so $\theta_3\rightarrow\tilde{\theta}_3$ and $\omega_3\rightarrow 0$ within the neighbourhood of E_2.

In order to simulate the transition from E_1 to E_2 a small perturbation of the state variable is used to begin the transition towards E_2. The transition from E_1 to E_2 can be seen in Fig. 5, where the controller ensures capture and stabilisation at E_2. The corresponding control time history is shown in Fig. 6, which uses κ_2 as the control with fixed κ_1 while the corresponding geometry of the transition process can be seen in Fig. 7. These results demonstrate that the controller can compensate for errors to generate a path between two unstable equilibrium points for this simple rigid bar system.

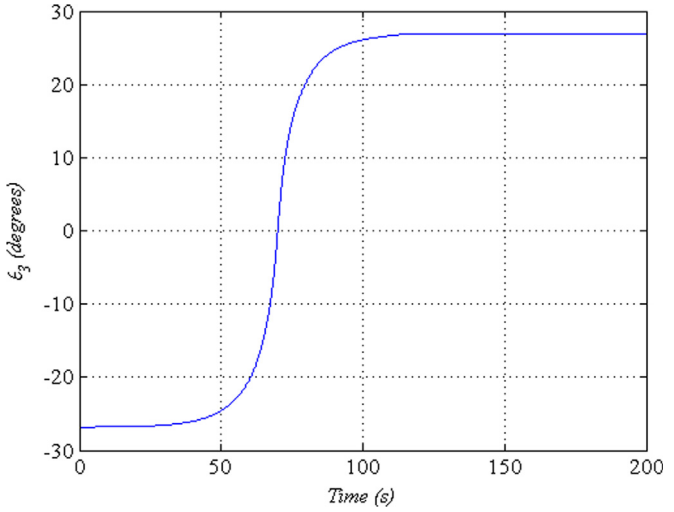

Fig. 5. Variation of θ_3 during the transition from E_1 to E_2.

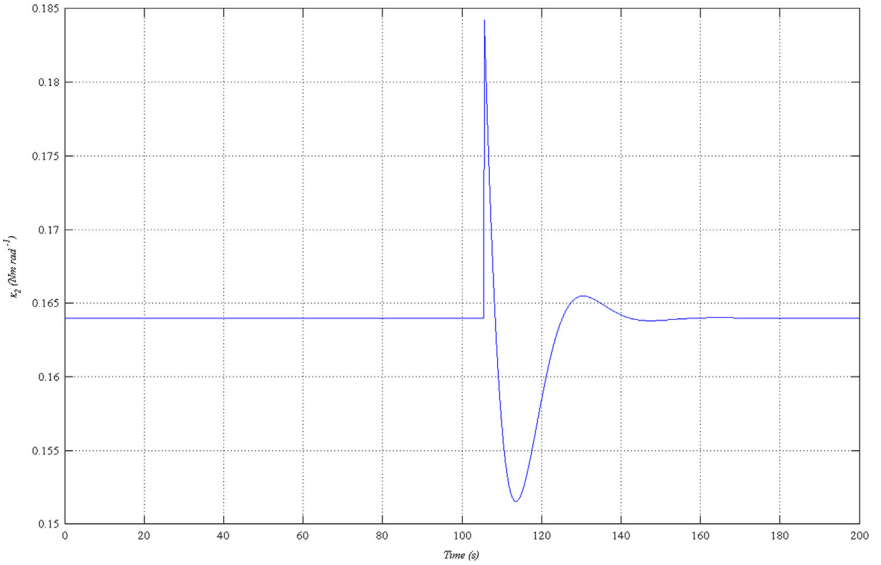

Fig. 6. Control in the neighbourhood of E_2 actuated through the parameter κ_2.

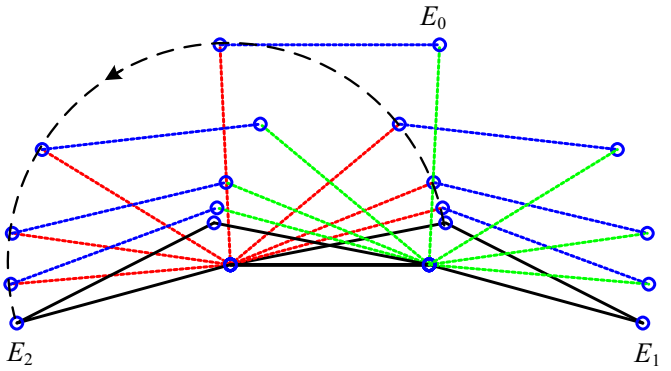

Fig. 7. Kinematics of the transition process.

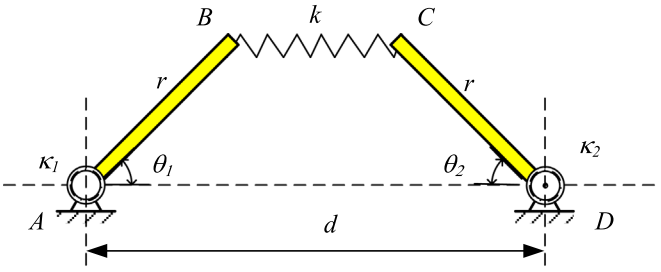

Fig. 8. Pseudo-rigid model with a single axial spring.

3. Pseudo-rigid four-bar model

Building on the rigid four-bar mechanism from Section 2, an approximate flexible model can now be considered to investigate the effect of elastic bars, shown in Fig. 8. The middle rigid bar is now substituted by an axial spring with two torsional springs now at both ends.

3.1. Pseudo-rigid model

Due to the elastic bar, the pseudo-rigid four-bar mechanism is now a two degree-of-freedom system. Two angles are now utilised as the state variables, and the torsional springs used as controllers. If the angles of the two rigid bars are defined by $\boldsymbol{\theta}$ (θ_1, θ_2), while the span of the mechanism is d and the length of each rigid bar is r, as shown in Fig. 8, it can be demonstrated that the axial spring has length$l$, which with deformation, is given by

$$l=\sqrt{\left(d - r\left(\cos\theta_1 + \cos\theta_2\right)\right)^2 + \left(r\left(\sin\theta_1 - \sin\theta_2\right)\right)^2} \tag{15}$$

Firstly, the model is again considered to be a conservative system with the simplification that it has unit mass. The free parameters of the model are now the axial spring stiffness k and natural length l_0, the torsional spring stiffness$\boldsymbol{\kappa}(\kappa_1, \kappa_2)$ and initial (undeflected) angles θ_{10},θ_{20}. The Hamiltonian for this model can be defined from the kinetic energy and potential energy with a simplification of unit moment of inertia through Eqs. (16) and (17) as

$$T(\boldsymbol{\omega})=\frac{1}{2}\left(\omega_1^2\right)+\frac{1}{2}\left(\omega_2^2\right) \tag{16}$$

$$V(\boldsymbol{\theta}, \boldsymbol{\kappa})=\frac{1}{2}\kappa_1\left(\theta_1 - \theta_{10}\right)^2+\frac{1}{2}\kappa_2\left(\theta_2 - \theta_{20}\right)^2+\frac{1}{2}k\left(l-l_0\right)^2 \tag{17}$$

with angular velocity coordinates are ω_1 and ω_2. We can now fully define the problem by a dynamical system of the form

$$\dot{\theta}_1=\omega_1 \tag{18}$$

$$\dot{\omega}_1= -\kappa_1\left(\theta_1-\theta_{10}\right)-k\left(l-l_0\right)\frac{dl}{d\theta_1} \tag{19}$$

$$\dot{\theta}_2=\omega_2 \tag{20}$$

$$\dot{\omega}_2= -\kappa_2\left(\theta_2-\theta_{20}\right)-k\left(l-l_0\right)\frac{dl}{d\theta_2} \tag{21}$$

Here, the aim of the pseudo-rigid model is to understand how heteroclinic connections can be found for a two-degree-of-freedom system, to enable such connections to be found for the fully elastic model in Section 4. Therefore, in order to capture the essential dynamics of the model, but to keep the model tractable, Taylor expansions are used to substitute for

Table 3
Equilibrium points with corresponding potential energy.

Point	θ_1	θ_2	V	$D\,(1\times10^{-6})$	Type
E_0	0	0	1.25	0.9047	Stable
E_1	44.38	44.3811	0.8	−0.1705	Unstable
E_2	−44.38	−44.3811	0.8	−0.1705	Unstable
E_3	−34.11	34.1116	0.4278	0.3932	Stable
E_4	34.11	−34.1116	0.4278	0.3932	Stable

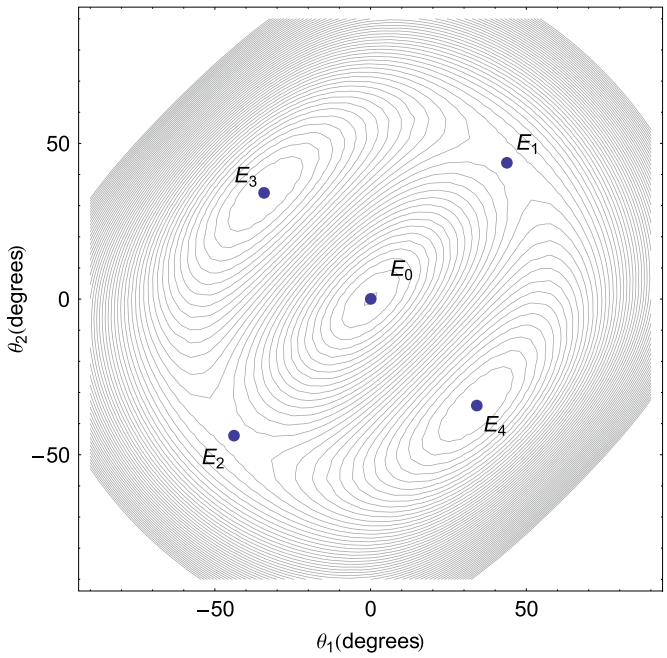

Fig. 9. Potential $V(\boldsymbol{\theta}, \boldsymbol{\kappa})$ and equilibria (3 unstable equilibria E_0, E_1 and E_2, and 2 stable equilibria E_3 and E_4).

trigonometric function using Eqs. (22) and (23) as

$$\sin\theta = \theta - \frac{\theta^3}{6} + o\left(\theta^5\right) \tag{22}$$

$$\cos\theta = 1 - \frac{\theta^2}{2} + o\left(\theta^4\right) \tag{23}$$

Then, dynamical system theory can be used to investigate the characteristics of this simplified smart structure model [22]. It will be shown that the system defined by Eqs. (18)–(21) has a number of equilibria which are both stable and unstable and may be connected in the phase space of the problem. Again, heteroclinic connections can be found which requires that the stable and unstable manifolds of the two unstable equilibria are connected. Solving Eqs. (19) and (21) for equilibrium conditions yields five equilibria for the parameter set, $\kappa_1 = \kappa_2 = \kappa = 1$ N m/rad, $d = 15$ cm, $l_0 = 10$ cm, $r = 5$ cm, $k = 1$ N/m. The location of the equilibria are listed in the Table 3.

Then, the Hessian matrix of the potential energy can be used to test the linear stability properties of these equilibria. In the second derivative test for determining extrema of the potential function $V(\boldsymbol{\theta}, \boldsymbol{\kappa})$, the discriminant D is given by

$$D = \begin{vmatrix} \dfrac{\partial^2 V}{\partial\theta_1^2} & \dfrac{\partial^2 V}{\partial\theta_1\partial\theta_2} \\ \dfrac{\partial^2 V}{\partial\theta_2\partial\theta_1} & \dfrac{\partial^2 V}{\partial\theta_2^2} \end{vmatrix} \tag{24}$$

According to the second derivative test discriminant, it can be determined that the system possesses 1 unstable equilibrium point E_0, where the potential has a global maximum, 2 unstable equilibria E_1–E_2 where the potential has a saddle and 2 stable equilibria E_3–E_4 where the potential has a global minimum, as can be seen in Fig. 9.

3.2. Numerical solution

In previous work heteroclinic connections were used to reconfigure a simple smart structure model between two unstable equilibria which lie on the same energy surface [16]. In principle, the structure could be reconfigured between these two unstable equilibria without work being done. To find heteroclinic connections, dynamical theory can be used with Eqs. (18)–(21) firstly linearised in the neighbourhood of each equilibrium point to yield their associated eigenvalues and eigenvectors. These stable and unstable eigenvectors $\mathbf{u}^{\mathrm{s}}$ and $\mathbf{u}^{\mathrm{u}}$ are tangent to the stable manifold $\boldsymbol{W}_{\mathrm{s}}$ and the unstable manifold $\boldsymbol{W}_{\mathrm{u}}$ corresponding to the eigenvalues $\lambda = -1$ and $\lambda = +1$, respectively. Therefore, integrating forwards or backwards from an unstable equilibrium point, the eigenvectors can be mapped to approximate the stable and unstable manifolds. The initial conditions in the neighbourhood of each equilibrium point $\boldsymbol{t}^{\boldsymbol{e}} = (\tilde{\boldsymbol{\theta}}, 0)$ for forward and backward

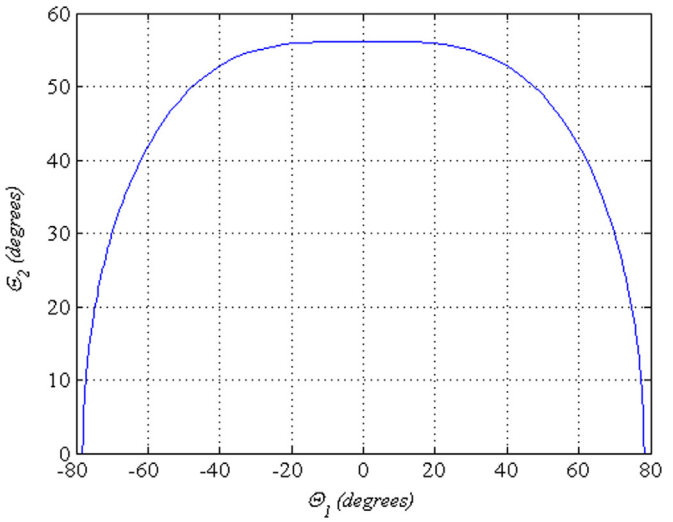

Fig. 10. Heteroclinic connection between E_1 and E_2 with the projection of the phase space onto the configuration space shown (note the perpendicular crossing of Θ_1=0).

integration can be defined as

$$\boldsymbol{t}^{s}=\boldsymbol{t}^{e}+\epsilon\boldsymbol{u}^{s} \tag{25}$$

$$\boldsymbol{t}^{u}=\boldsymbol{t}^{e}+\epsilon\boldsymbol{u}^{u} \tag{26}$$

for $\epsilon \ll 1$, $\boldsymbol{t}=(\boldsymbol{\theta}, \boldsymbol{\omega}) \in \mathbf{R}^4$ and where $\tilde{\boldsymbol{\theta}}$corresponds to the location of the appropriate equilibrium point.

Due to the sensitivity of the problem, phase trajectories emerging from one unstable equilibrium point will not reach the other unstable equilibrium precisely. To compensate, the symmetry of the problem can be used to search for an accurate heteroclinic connection. The symmetric case $\kappa_1=\kappa_2=\kappa$ will now be considered so that the ratio κ/k can be manipulated to find an ideal heteroclinic connection. Considering the symmetry of the problem, a coordinate transformations can be used to rotate the coordinate axes (θ_1, θ_2) anticlockwise

$$\begin{pmatrix}\theta_1\\ \theta_2\end{pmatrix}=\frac{1}{\sqrt{2}}\begin{pmatrix}1 & -1\\ 1 & 1\end{pmatrix}\begin{pmatrix}\Theta_1\\ \Theta_2\end{pmatrix} \tag{27}$$

In this new coordinate system, the equations of motion can be obtained to find a heteroclinic connection [16]. The system is now symmetric about the axes Θ_1=0 and Θ_2=0 and the unstable manifold of E_1 is the symmetric with the stable manifold of E_2. Therefore, a heteroclinic connection between E_1 and E_2 must be perpendicular to the Θ_1=0 axis, which means $\dot{\Theta}_2$=0 (or less than some cut-off) on crossing the axis and so the heteroclinic connection will have a mirror image under $\Theta_2 \rightarrow -\Theta_2$, as shown in Figs. 10 and 11.

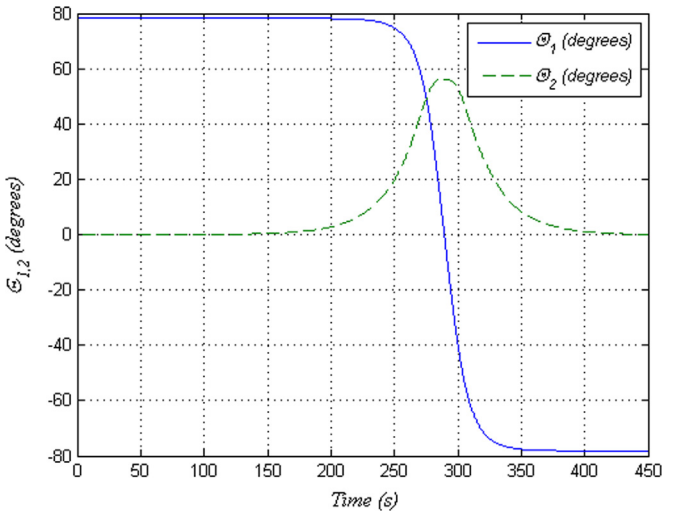

Fig. 11. Transformed coordinates Θ_1 and Θ_2 for a heteroclinic connection between E_1 and E_2.

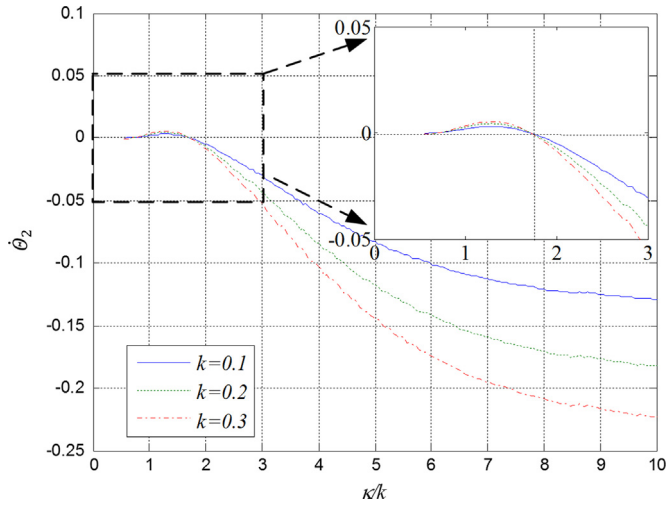

Fig. 12. Value of $\dot{\theta}_2$ at the first crossing of the unstable manifold of E_1 with the θ_2 axis, with increasing parameter ratio κ/k.

Numerically, it is found that for $\kappa/k<1$, $\dot{\theta}_2$ is sufficiently small for an approximate heteroclinic connection to exist, as shown is Fig. 12. Then when $\kappa/k\approx1.7$, a heteroclinic connection exists, irrespective of the value of k, as is clearly seen in Fig. 12. This demonstrates that for each value of k there is a value of κ which admits a heteroclinic connection. The heteroclinic connection can also be seen in Figs. 13 and 14, which is shown in the original untransformed coordinate axes (θ_1, θ_2).

While this method is suitable for the relatively low order problem represented by the pseudo-rigid four-bar model, other methods must now be sought for the more complex fully-elastic four-bar model.

4. Fully-elastic four-bar model

4.1. Modelling and analysis

In order to further explore the possibility of reconfiguring smart structures using heteroclinic connections, a more complex fully elastic model will now be considered, building on the two-degree-of-freedom model in Section 3. A buckled beam is now assumed to be divided into three linear axial springs with unit mass and four torsional springs considered, as shown in Fig. 15. While this represents a fully elastic model of the four-bar mechanism, it also clearly represents an approximate model of a buckling beam. It has been shown that the former model in Section 3 admits families of heteroclinic connections in the phase space of the problem. This more complex problem greatly increases the number of equilibria in the

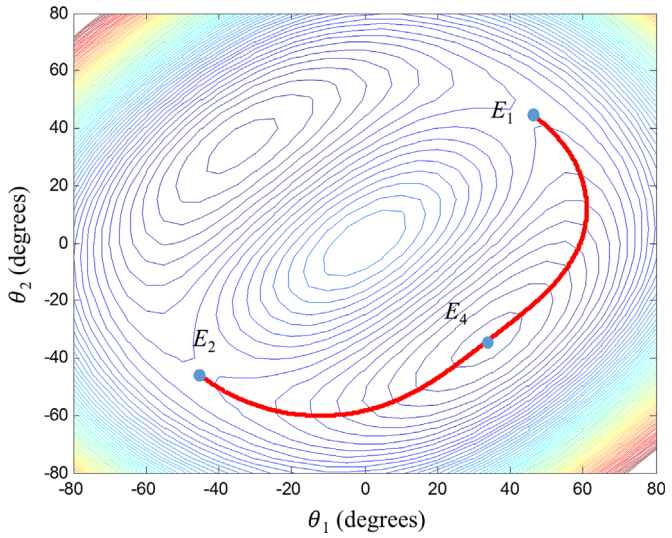

Fig. 13. Uncontrolled heteroclinic connection between E_1 and E_2 in the original untransformed coordinate axes (θ_1, θ_2).

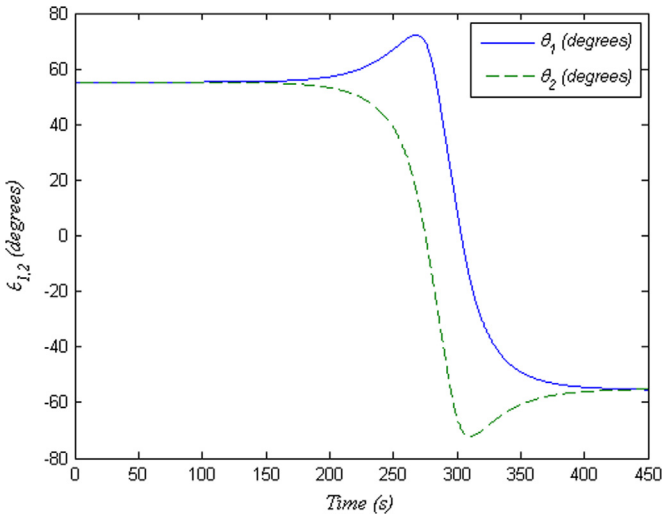

Fig. 14. Untransformed coordinates θ_1 and θ_2 for an uncontrolled heteroclinic connection between E_1 and E_2.

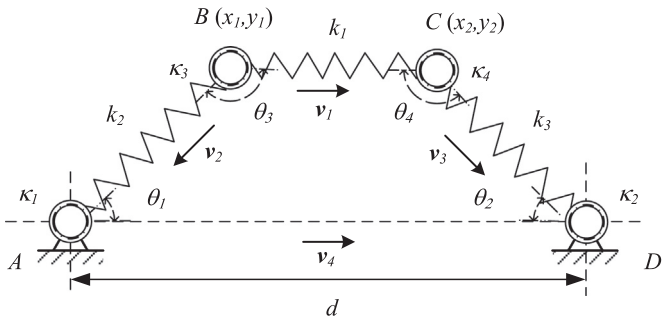

Fig. 15. Fully elastic four-bar mechanism/buckling beam model.

system and the difficulty of finding all exact equilibria by purely numerical means. Only a subset of the large number of equilibria will therefore be used to illustrate the properties of the system and seek heteroclinic connections between two unstable equilibria.

In Fig. 15, the distance between two ends of the structure is denoted by d. The length of the three springs are denoted by l_1, l_2 and l_3 with corresponding stiffness k_1, k_2 and k_3 respectively. Considering each of these springs as links, θ_1 and θ_2 are the angles of spring 2 and spring 3 with respect to the horizontal with torsional stiffness κ_1 and κ_2. Finally, θ_3 and θ_4 are the angles of spring 2 and spring 3 respect to spring 1 with the torsional stiffness $\kappa_3$and κ_4. This new model of a flexible four-bar link is a four degree-of-freedom system with two constrained points B (x_1, y_1) and C (x_2, y_2), with A the origin point. The angles can therefore be defined as

$$\theta_1=\tan^{-1}\frac{y_1}{x_1} \tag{28}$$

$$\theta_2=\tan^{-1}\frac{y_2}{d-x_2} \tag{29}$$

$$\theta_3=\cos^{-1}(\boldsymbol{v}_1, \boldsymbol{v}_2) \tag{30}$$

$$\theta_4=\cos^{-1}(-\boldsymbol{v}_1, \boldsymbol{v}_3) \tag{31}$$

where $\boldsymbol{v}_1$, $\boldsymbol{v}_2$ and $\boldsymbol{v}_3$ denote the axial direction vectors of the springs, as shown in Fig.15. The deformation of the springs can therefore be defined as

$$\Delta l_1=|\boldsymbol{v}_1|-l_1 \tag{32}$$

$$\Delta l_2=|\boldsymbol{v}_2|-l_2 \tag{33}$$

$$\Delta l_3=|\boldsymbol{v}_3|-l_3 \tag{34}$$

Again, this fully elastic model is considered to be a conservative system. The potential energy can then be defined as

$$V = \frac{1}{2}\kappa_1\theta_1^2+\frac{1}{2}\kappa_2\theta_2^2+\frac{1}{2}\kappa_3\theta_3^2+\frac{1}{2}\kappa_4\theta_4^2+\frac{1}{2}k_1\Delta l_1^2+\frac{1}{2}k_2\Delta l_2^2+\frac{1}{2}k_3\Delta l_3^2 \tag{35}$$

where κ is the torsional spring constant, k is the axial spring constant.

Established methods can now be employed to select the appropriate spring constants for the model using geometric and material parameters, according to the following [23]

$$\kappa=\frac{2EI}{l_{eff}} \tag{36}$$

$$k=\frac{CAE}{l} \tag{37}$$

where E is the equivalent elastic modulus, I is the equivalent cross-sectional moment of inertia, l_{eff} is an effective length, A is the equivalent cross-sectional area and l is length of the axial spring. Eqs. (36) and (37) present a direct relationship between the basic material parameters of a continuous beam and the model parameters so that it is possible to construct a practical purely elastic model with the actual material parameters. The potential energy can then be defined as a function of E,l_{eff} as

$$V=f\left(E, l_{eff}, l\right) \tag{38}$$

for some functional relationship f. Eq. (38) provides a relationship between the potential energy and basic material properties, so that these parameters can be selected to construct a reasonable fully elastic model as described in Section 4.2 below.

4.2. Euler–Bernoulli beam model

The Euler–Bernoulli equations for an elastic buckled beam are now used to evaluate the spring model discussed above. It is known that the first and second buckling shapes are given by

$$y_1=a_1\left(1-\cos\left(2\pi\frac{x}{L}\right)\right) \tag{39}$$

and

$$y_2=a_2\left(1-2\pi\frac{x}{L}-\cos\left(N\frac{x}{L}\right)+\frac{2}{N}\sin\left(N\frac{x}{L}\right)\right) \tag{40}$$

respectively, where N is the first positive solution to $\tan(N/2)=N/2$ and a_1 and a_2 are constants which can be determined through the method discussed in Ref. [24]. Note that the y is the displacement of a beam element from the x-axis.

Although more mode shapes could be used, the first two buckling modes provide a good approximation. Fig. 16 depicts the first two modes of the buckled beam for each model shape corresponding to positive (solid line) and negative (dash line) values of a_1 and a_2.

The Euler–Bernoulli can now be used to optimise the selection of the free parameters of the model to best represent a true buckling beam.

4.3. Energy analysis [25]

The deformation energy of the beam will now be used to compare the approximation between the Euler–Bernoulli beam model with the elastic beam model of Section 3.1. This deformation energy is defined in Cartesian coordinates and includes

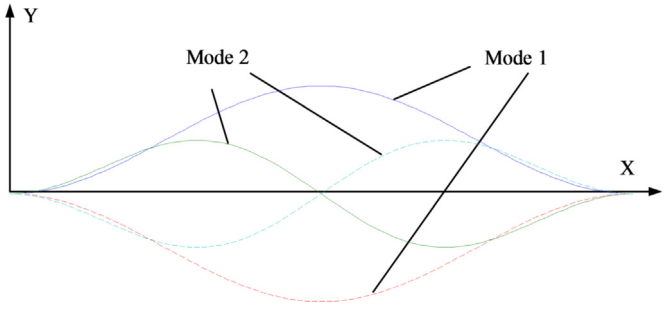

Fig. 16. Buckling modes of a clamped – clamped buckling beam.

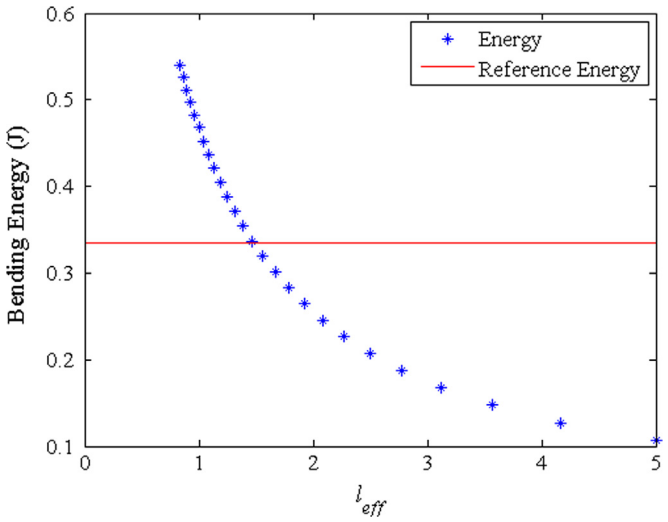

Fig. 17. Bending energy based on effective length which is used to approximate the torsional springs.

two parts, the bending energy and the compression energy. The bending energy of the Euler–Bernoulli beam is defined by

$$U_b \simeq \frac{EI}{2}\int_0^L y''(x)^2 dx \tag{41}$$

where I is the area moment of inertia of the beam, L is the compressed beam length (distance between clamping points), E is the modulus of elasticity, x is the horizontal axis distance along the beam and y is the beam vertical displacement.

The compressive energy in the beam can be calculated directly from Hooke's Law as

$$U_c = \frac{AE\left[2(L-L_0) + \int_0^L y'(x)^2 dx\right]^2}{8L_0^2} \tag{42}$$

where A is the cross-sectional area of the beam and L_0 is the undeformed beam length.

Returning to Eq. (36), we can seek a more accurate elastic spring model through comparison with the Euler–Bernoulli model. Therefore, the purely elastic model can be modified by changing the effective length l_{eff} to matching the potential energy which is calculated in the Euler–Bernoulli model. Fig. 17 depicts the bending energy with increasing effective length, while the red line is the energy of the first mode of the Euler beam model. From Fig. 17, the approximate value of the effective length can be selected as 1.7, which will be used to define a modified fully elastic model.

The comparison between the elastic spring model and the Euler–Bernoulli is shown in Fig. 18 for the energy of each mode, where it can be seen that the first mode error is smaller than the second mode error. The deformation energy error of

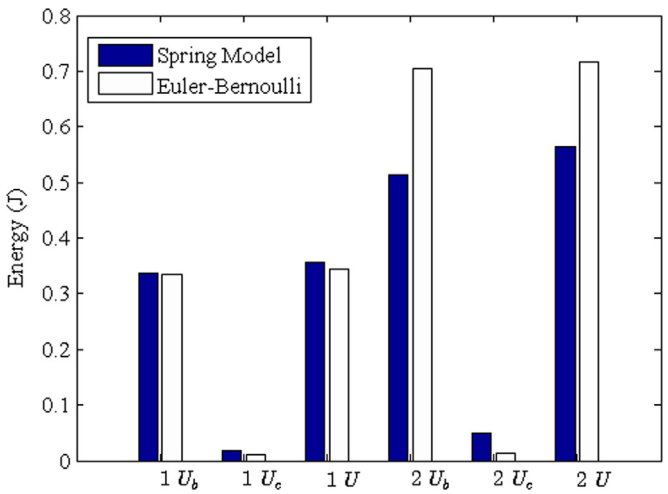

Fig. 18. Energy comparison between the fully elastic spring model and Euler–Bernoulli beam model. U_b is the bending energy, U_c is the compressive energy, $U=U_b+U_c$.

the first mode is approximately 3%, while the deformation energy error of second mode is approximately 17%. Therefore, the fully elastic spring model can be considered as a simplified model for a continuous beam with relatively accurate approximation.

4.4. Numerical validation

In order to explore the possibility of reconfiguring this new model, dynamical system theory can again be used to investigate its characteristics. Firstly, the model is again considered to be a conservative system with the assumption of unit mass. From Fig. 15, the Hamiltonian for this two mass model can then be defined from the kinetic and potential energy through Eqs. (43) and (44) as

$$T(\boldsymbol{p})=\frac{1}{2}(x_1^2)+\frac{1}{2}(x_2^2)+\frac{1}{2}(y_1^2)+\frac{1}{2}(y_2^2) \tag{43}$$

$$V(\boldsymbol{x},\boldsymbol{L})=\frac{1}{2}\begin{bmatrix}\kappa_1 & \kappa_2 & \kappa_3 & \kappa_4\end{bmatrix}\begin{bmatrix}\theta_1^2\\ \theta_2^2\\ \theta_3^2\\ \theta_4^2\end{bmatrix}+\frac{1}{2}\begin{bmatrix}k_1 & k_2 & k_3\end{bmatrix}\begin{bmatrix}l_1^2\\ l_2^2\\ l_3^2\end{bmatrix}=h(x_1,x_2,y_1,y_2) \tag{44}$$

Now it can be described by a Hamiltonian $H(\boldsymbol{x},\boldsymbol{p},\boldsymbol{L})=T(\boldsymbol{p})+V(\boldsymbol{x},\boldsymbol{L})$ with the set $\boldsymbol{x}=\{x_1,x_2,y_1,y_2\}$ and the corresponding set of momentum $\boldsymbol{p}=\{p_1,p_2,p_3,p_4\}$. We can now fully define the problem by a dynamical system of the form

$$\dot{\boldsymbol{x}}=\boldsymbol{p} \tag{45}$$

$$\dot{\boldsymbol{p}}=\boldsymbol{g}(x_1,x_2,y_1,y_2) \tag{46}$$

with momentum coordinates $\boldsymbol{p}$ and for some functional relationship$\boldsymbol{g}$. It will be shown that the system defined by Eqs. (45) and (46) again has a large number of equilibria which are both stable and unstable and may be connected in the phase space of the problem. Although there are many equilibria in the system, considering the complexity of the problem (with trigonometric functions), it is difficult to locate all of the equilibria. Therefore an optimisation algorithm is now used to find some typical equilibria which are denoted as equivalent to the first mode and second mode of an Euler–Bernoulli beam, as shown in Fig. 19.

Linearisation of Hamilton's equations in the neighbourhood of each equilibrium point can now be used to determine the linear stability of these equilibria according to their eigenvalues λ_j(j = 1 − 8). A set of stable equilibria are expected with conjugate imaginary eigenvalues and a set of unstable equilibria are expected with real eigenvalues of opposite sign [22]. The corresponding parameters can be seen from Table 4 where E_0 is an unstable equilibrium, where the potential has a global maximum; E_1 and E_2 are stable equilibria where the potential has a local minimum; E_3 and E_4 are unstable equilibria where the potential has saddles.

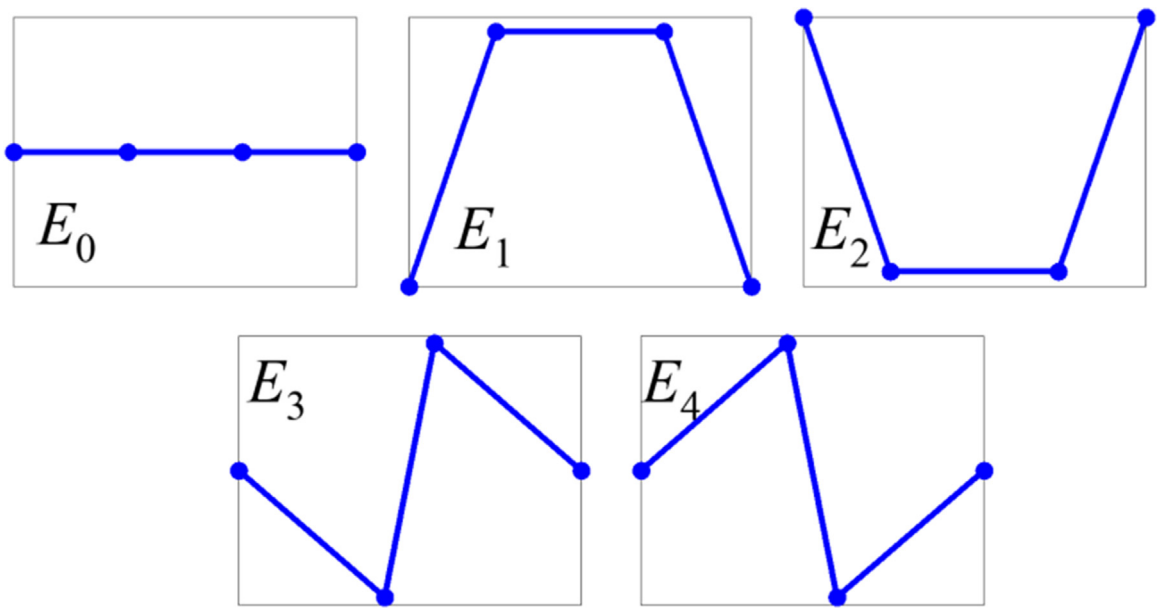

Fig. 19. Corresponding shape of fully elastic model in equilibrium positions.

Table 4
Stability properties of the 5 equilibria of the fully elastic model.

Points	E_0	E_1	E_2	E_3	E_4
x_1	3.33	2.64	2.64	4.07	4.07
y_1	0	4.07	−4.07	−2.20	2.20
x_2	6.67	7.36	7.36	5.93	5.93
y_2	0	4.07	−4.07	2.20	−2.20
$\lambda_{1,2}$	$\pm 0.95i$	$\pm 0.86i$	$\pm 0.86i$	$\pm 0.77i$	$\pm 0.77i$
$\lambda_{3,4}$	$\pm 0.55i$	$\pm 0.54i$	$\pm 0.54i$	$\pm 0.55i$	$\pm 0.55i$
$\lambda_{5,6}$	± 0.54	$\pm 0.14i$	$\pm 0.14i$	$\pm 0.55i$	$\pm 0.55i$
$\lambda_{7,8}$	± 0.35	$\pm 0.40i$	$\pm 0.40i$	± 0.096	± 0.096
V	1.25	0.36	0.36	0.56	0.56
Type	Saddle	Min	Min	Saddle	Max

Since the Hamiltonian of the system is constant, and formed by the potential and kinetic energy V and T, the volume of phase space in $\mathbf{R}^8$, and its projection to configuration space in $\mathbf{R}^4$, is constrained by the requirement that $\boldsymbol{T}(p) > 0$. Since the unstable equilibria E_3 and E_4 lie on the same energy surface, we can assume that in principle a heteroclinic connection between these two equilibria may exist so that the structure can be reconfigured between them without work being done. Again in the absence of dissipation, the change in energy for the reconfiguration $\delta V \approx 0$.

The system is strongly nonlinearity so that it is difficult to find heteroclinic connections using the direct method presented in Section 3.2. Therefore, we employ an optimisation method to find a suitable parameter set. An objective function is constructed in Eq. (47), the minimisation of which provides the requirement for a heteroclinic connection.

$$F = (\dot{y}_1 + \dot{y}_2)^2 + \left((\dot{x}_1, \dot{x}_2) \bullet (x_1 - x_{10}, x_2 - x_{20}) \right)^2 \tag{47}$$

Therefore, for a heteroclinic connection between E_3 and E_4, if one exists, the symmetry property requires that Eq. (47) vanishes. We integrate the system of equations in the direction of the unstable eigenvector of E_3 as in Eq. (26), until it intersects the symmetry axis y_1–y_2=0, i.e. y_1=y_2, and we measure the six states $\dot{x}_1$, $\dot{x}_2$,$\dot{y}_1$,$\dot{y}_2$,x_1,x_2. Through substitution of these values into Eq. (47), the value of the objective function can be calculated. Then the condition $(\dot{y}_1+\dot{y}_2)$=0guarantees that the trajectory is perpendicular to the symmetry axis y_1–y_2, and $((\dot{x}_1, \dot{x}_2)\bullet(x_1-x_{10}, x_2-x_{20}))$ expresses the dot product of two vectors that ensure the projection of the heteroclinic connection is symmetric in x_1–x_2.

Again, due to the sensitivity of the problem, and in a real smart structure parameter errors, phase trajectories emerging from one unstable equilibrium point will not reach the other unstable equilibrium precisely, which means Eq. (47) cannot obtain a precise set of parameters using the optimisation method. To compensate for such errors, the active control method which was used in Section 3 is again used to capture phase space trajectories in a neighbourhood of the target unstable equilibrium point. The transition from E_3 to E_4 can be seen in Fig. 20, where the controller ensures capture and stabilisation at E_4. The connection in the coordinate space x_1–x_2 can be seen as a homoclinic connection, and in the coordinate space y_1–y_2 can be seen as a heteroclinic connection. The transition can also be seen in Fig. 21, which provides the time history of the four state variables. The corresponding controls κ_1, κ_2, $k_1$and k_2 are shown in Fig. 22. Fig. 23 shows the geometry of the transition process. The closed dotted line indicates the midpoint of the transition.

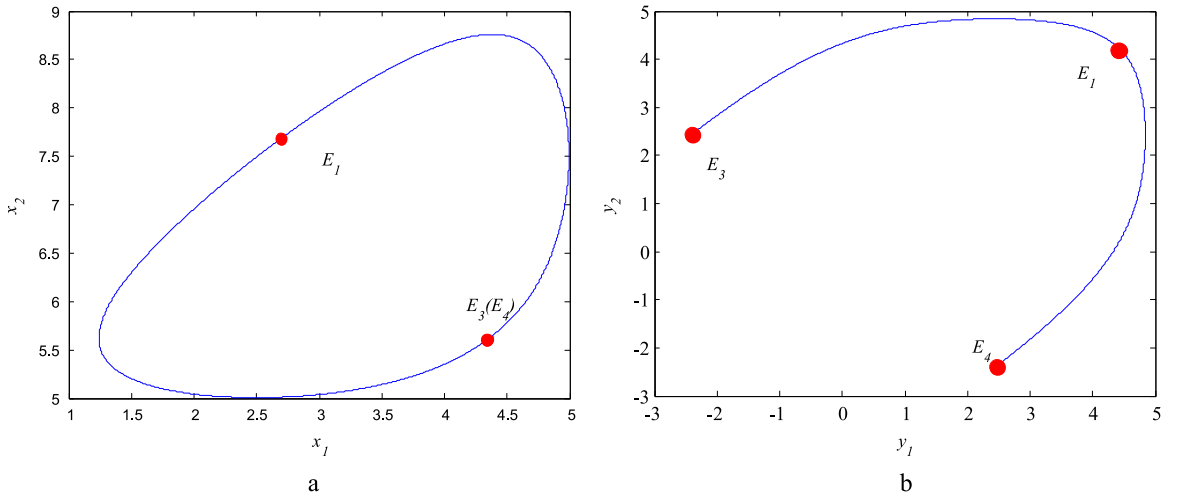

Fig. 20. Controlled transition from E_3 to E_4 with the controller active in the neighbourhood of E_4. (a) Homoclinic connection in the x_1–x_2 coordinate space, (b) Heteroclinic connection in the y_1–y_2 coordinate space.

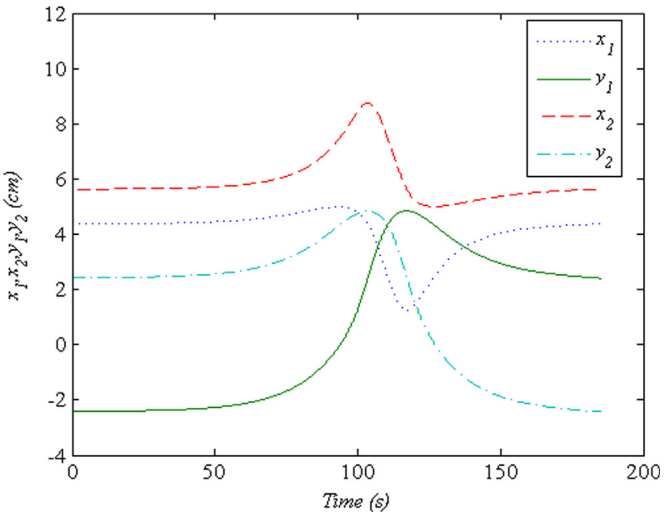

Fig. 21. Displacements during the transition from E_3 to E_4.

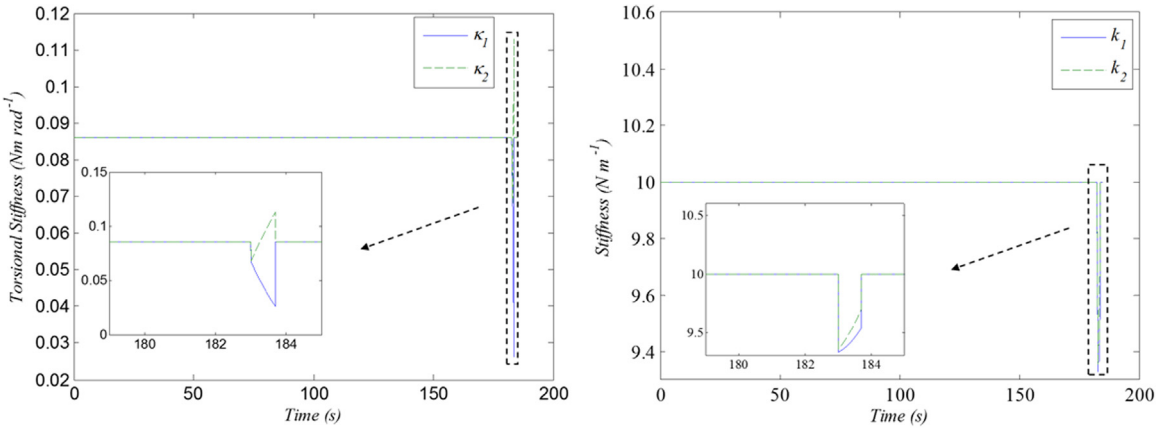

Fig. 22. Controls actuated at the end of the transition. (a) torsional spring stiffness, (b) axial spring stiffness.

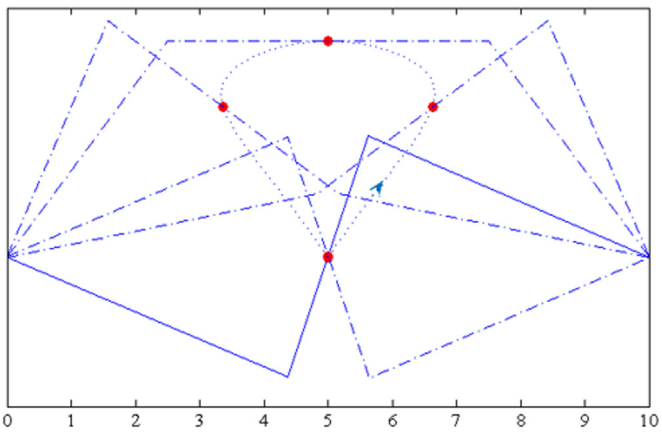

Fig. 23. Geometry of the transition process where the red point is the mid-point of the structure, which has a trajectory shown as a dashed line. (For interpretation of the references to colour in this figure legend, the reader is referred to the web version of this article.)

5. Conclusions

Using the kinematic theory of mechanisms, an analysis has been firstly been presented regarding the reconfiguration of a simple four-bar linkage through heteroclinic connections. Then, a pseudo-rigid model was developed as an unstable structure which has several equilibria (stable and unstable), again with heteroclinic connections found. In principle, such reconfigurations do not require the input of energy, unlike transitions between stable equilibria which required the addition of and the dissipation of energy. Finally, the reconfiguration method has been used to investigate the behaviour of a more realistic elastic smart structure model. By comparing the deformation energy of the elastic spring model and a truly continuous model, it can be verified that the spring model can provide a good approximation to a buckling beam. This more complex dynamical model, which has strong nonlinearity, can again be reconfigured through transitions between unstable equilibria.

References

[1] A.G. Erdman., G.N. Sandor., Mechanism Design: Analysis and Synthesis, vol. 1, Prentice-Hall, Inc, London, U.K, 1997.
[2] P.G. Opdahl, B.D. Jensen, L.L. Howell, An investigation into compliant bistable mechanisms, in: Proceedings of the ASME Des. Eng. Tech. Conf., Atlanta, GA.
[3] T.M. Pendleton, B.D. Jensen, Development of a tristable compliant mechanism, in: Proceedings of the 12th World Congr. Mech. Mach. Sci., Besancon, France.
[4] M.P. Brenner, J.H. Lang, J. Li, J. Qiu, A.H. Slocum, Optimal design of a bistable switch, Proc. Natl. Acad. Sci. USA 100 (2003) 9663–9667, http://dx.doi.org/10.1073/pnas.1531507100.
[5] M. Takenaka, M. Raburn, Y. Nakano, All-optical flip-flop multimode interference bistable laser diode, IEEE Photonics Technol. Lett. 17 (2005) 968–970, http://dx.doi.org/10.1109/LPT.2005.844322.
[6] T. Lebar, U. Bezeljak, A. Golob, M. Jerala, L. Kadunc, B. Pirš, et al., A bistable genetic switch based on designable DNA-binding domains, Nat. Commun. 5 (2014) 5007, http://dx.doi.org/10.1038/ncomms6007.
[7] B. Camescasse, A. Fernandes, J. Pouget, Bistable buckled beam: elastica modeling and analysis of static actuation, Int. J. Solids Struct. 50 (2013) 2881–2893, http://dx.doi.org/10.1016/j.ijsolstr.2013.05.005.
[8] B. Camescasse, A. Fernandes, J. Pouget, Bistable buckled beam and force actuation: experimental validations, Int. J. Solids Struct. 51 (2014) 1750–1757, http://dx.doi.org/10.1016/j.ijsolstr.2014.01.017.
[9] J. Cleary, H.-J. Su, Modeling and experimental validation of actuating a bistable buckled beam via moment input, J. Appl. Mech. 82 (2015) 051005, http://dx.doi.org/10.1115/1.4030074.
[10] J.L. Silverberg, J.-H. Na, A.A. Evans, B. Liu, T.C. Hull, C.D. Santangelo, et al., Origami structures with a critical transition to bistability arising from hidden degrees of freedom, Nat. Mater. 14 (2015) 389–393, http://dx.doi.org/10.1038/nmat4232.
[11] S. Daynes, A. Grisdale, A. Seddon, R. Trask, Morphing structures using soft polymers for active deployment, Smart Mater. Struct. 23 (2014) 012001, http://dx.doi.org/10.1088/0964-1726/23/1/012001.
[12] D.C. Lagoudas, Shape Memory Alloys: Modeling and Engineering Applications, Springer, New York, 2008.
[13] A.B. Flatau, K.P. Chong, Dynamic smart material and structural systems, Eng. Struct. 24 (2002) 261–270, http://dx.doi.org/10.1016/S0141-0296(01)00093-1.
[14] T. Hogg, B.A. Huberman, Controlling smart matter, Smart Mater. Struct. 7 (1998) R1–R14, http://dx.doi.org/10.1088/0964-1726/7/1/001.
[15] S. Felton, M. Tolley, E. Demaine, D. Rus, R. Wood, A method for building self-folding machines, Science 345 (2014) 644–646, http://dx.doi.org/10.1126/science.1252610. (80-.).
[16] C.R. McInnes, T.J. Waters, Reconfiguring smart structures using phase space connections, Smart Mater. Struct. 17 (2008) 025030, http://dx.doi.org/10.1088/0964-1726/17/2/025030.
[17] O. Guenther, T. Hogg, B.A. Huberman, Controls for unstable structures, in: Smart Struct. Mater. 1997 Math. Control Smart Struct. Soc. Photo-Optical Instrum. Eng. Conf. (June); Proc.SPIE, 1997: pp. 754–763. ⟨http://dx.doi.org/10.1117/12.276594⟩.
[18] C.R. McInnes, D.G. Gorman, M.P. Cartmell, Enhanced vibrational energy harvesting using nonlinear stochastic resonance, J. Sound Vib. 318 (2008) 655–662, http://dx.doi.org/10.1016/j.jsv.2008.07.017.
[19] J. Zhang, C.R. McInnes, Reconfiguring smart structures using approximate heteroclinic connections in a spring-mass model, in: Proceedings of the ASME Conf. Smart Mater. Adapt. Struct. Intell. Syst. (SMASIS 2015), Colorado Springs, 2015.
[20] J. Zhang, C.R. McInnes, Reconfiguring smart structures using approximate heteroclinic connections, Smart Mater. Struct. 24 (2015) 105034, http://dx.doi.org/10.1088/0964-1726/24/10/105034.
[21] L.L. Howell, A. Midha, A method for the design of compliant mechanisms with small-length flexural pivots, J. Mech. Des. 116 (1994) 280, http://dx.doi.org/10.1115/1.2919359.
[22] S. Wiggins, Introduction to Applied Nonlinear Dynamical Systems and Chaos, Springer, New York, 1990.
[23] D.E. Vogtmann, S.K. Gupta, S. Bergbreiter, Characterization and modeling of elastomeric joints in miniature compliant mechanisms, J. Mech. Robot. 5 (2013) 041017, http://dx.doi.org/10.1115/1.4025298.
[24] S.P. Timoshenko, J.M. Gere, Theory of Elastic Stability, Dover Publications, Mineola, New York, 2009.
[25] Cazottes, Paul, et al., Bistable buckled beam: modeling of actuating force and experimental validations, Journal of Mechanical Design 131.10 (2009) 101001.